



**HAL**  
open science

## Identification of backgrounds in the EDELWEISS-I dark matter search experiment

S. Fiorucci, Alain Benoit, L. Berge, J. Blumer, A. Broniatowski, B. Censier, A. Chantelauze, M. Chapellier, G. Chardin, S. Collin, et al.

► **To cite this version:**

S. Fiorucci, Alain Benoit, L. Berge, J. Blumer, A. Broniatowski, et al.. Identification of backgrounds in the EDELWEISS-I dark matter search experiment. *Astroparticle Physics*, 2007, 28, pp.143-153. 10.1016/j.astropartphys.2007.05.003 . hal-00110250v2

**HAL Id: hal-00110250**

**<https://hal.science/hal-00110250v2>**

Submitted on 10 May 2007

**HAL** is a multi-disciplinary open access archive for the deposit and dissemination of scientific research documents, whether they are published or not. The documents may come from teaching and research institutions in France or abroad, or from public or private research centers.

L'archive ouverte pluridisciplinaire **HAL**, est destinée au dépôt et à la diffusion de documents scientifiques de niveau recherche, publiés ou non, émanant des établissements d'enseignement et de recherche français ou étrangers, des laboratoires publics ou privés.

# Identification of backgrounds in the EDELWEISS-I dark matter search experiment

The EDELWEISS Collaboration:

S. Fiorucci<sup>1,\*</sup>, A. Benoit<sup>2</sup>, L. Bergé<sup>3</sup>, J. Blümer<sup>4,5</sup>, A. Broniatowski<sup>3</sup>,  
 B. Censier<sup>3</sup>, A. Chantelauze<sup>5</sup>, M. Chapellier<sup>7</sup>, G. Chardin<sup>1</sup>, S. Collin<sup>3</sup>,  
 X. Defay<sup>3</sup>, M. De Jésus<sup>6</sup>, H. Deschamps<sup>1</sup>, P. Di Stefano<sup>6</sup>, Y. Dolgorouky<sup>3</sup>,  
 L. Dumoulin<sup>3</sup>, K. Eitel<sup>5</sup>, M. Fesquet<sup>1</sup>, J. Gascon<sup>6</sup>, G. Gerbier<sup>1</sup>, C. Goldbach<sup>8</sup>,  
 M. Gros<sup>1</sup>, M. Horn<sup>5</sup>, A. Juillard<sup>3</sup>, R. Lemrani<sup>1</sup>, A. de Lesquen<sup>1</sup>,  
 A. Lubashevskiy<sup>9</sup>, M. Luca<sup>6</sup>, S. Marnieros<sup>3</sup>, L. Mosca<sup>1</sup>, X.-F. Navick<sup>1</sup>,  
 G. Nollez<sup>8</sup>, E. Olivieri<sup>3</sup>, P. Pari<sup>7</sup>, V. Sanglard<sup>6</sup>, L. Schoeffel<sup>1</sup>, F. Schwamm<sup>1</sup>,  
 M. Stern<sup>6</sup>, E. Yakushev<sup>9</sup>

<sup>1</sup>CEA, Centre d'Études Nucléaires de Saclay, DSM/DAPNIA, 91191 Gif-sur-Yvette Cedex, France

<sup>2</sup>Centre de Recherche sur les Très Basses Températures, SPM-CNRS, BP 166, 38042 Grenoble, France

<sup>3</sup>Centre de Spectroscopie Nucléaire et de Spectroscopie de Masse, UMR8609 IN2P3-CNRS, Univ. Paris Sud, bât 108, 91405 Orsay Campus, France

<sup>4</sup>Institut für Experimentelle Kernphysik, Universität Karlsruhe (TH), Gaedestr. 1, 76128 Karlsruhe, Germany

<sup>5</sup>Forschungszentrum Karlsruhe, Institut für Kernphysik, Postfach 3640, 76021 Karlsruhe, Germany

<sup>6</sup>Institut de Physique Nucléaire de Lyon, Université de Lyon (Université Claude Bernard Lyon 1) et IN2P3-CNRS, 4 rue Enrico Fermi, 69622 Villeurbanne, France

<sup>7</sup>CEA, Centre d'Études Nucléaires de Saclay, DSM/DRECAM, 91191 Gif-sur-Yvette Cedex, France

<sup>8</sup>Institut d'Astrophysique de Paris, UMR7095 CNRS - Université Pierre et Marie Curie, 98 bis Bd Arago, 75014 Paris, France

<sup>9</sup>Laboratory of Nuclear Problems, JINR, Joliot-Curie 6, 141980 Dubna, Moscow Region, Russian Federation

## Abstract

This paper presents our interpretation and understanding of the different backgrounds in the EDELWEISS-I data sets. We analyze in detail the several populations observed, which include gammas, alphas, neutrons, thermal sensor events and surface events, and try to combine all data sets to provide a coherent picture of the nature and localization of the background sources. In light of this interpretation, we draw conclusions regarding the background suppression scheme for the EDELWEISS-II phase.

**PACS classification codes:** 95.35.+d, 14.80.Ly, 98.80.Es, 29.40.Wk.

\*Present address: Brown University, Department of Physics, Providence, RI 02912, USA

# 1 Introduction

EDELWEISS-I is the first phase of an experiment aiming at the direct detection of WIMPs (Weakly Interacting Massive Particles) which could constitute the dark matter halo of our Galaxy. It uses cryogenic detectors able to measure simultaneously the heat and ionization components of the energy deposit induced by the elastic scattering of a WIMP off a target nucleus (see e.g. [1] for a review).

The final analysis of the EDELWEISS-I data [2] covers a total fiducial exposure of 62 kg.d. The limits on the neutralino scattering cross-section were obtained from the observation of 40 nuclear recoil candidates with recoil energies between 15 and 200 keV, of which 3 are between 30 and 100 keV. The limits were obtained without the subtraction of any background, although the presence of a coincidence between two detectors and the study of charge collection distributions suggested that at least some of these events are due to a neutron background and surface interactions of electrons. In the preparation of the second phase of the experiment, it was necessary to perform a thorough investigation of all events in EDELWEISS-I before the nuclear recoil selection, in order to better assess their origin and devise means to remove as many background components as possible for EDELWEISS-II.

After a short description of the EDELWEISS-I experiment and of the active background rejection capabilities of heat/ionization cryogenic bolometers, this paper presents the evaluations of the backgrounds related to different origins : gamma radiation, alpha particles and other surface events, and neutrons. While the energy range of interest for WIMP detection is limited to below 100 keV, high energy gamma and alpha lines can prove very useful to understand the backgrounds in the range relevant to WIMP interactions.

## 2 EDELWEISS-I

### 2.1 General setup

EDELWEISS is located in the Laboratoire Souterrain de Modane (LSM) which provides a  $\sim 4800$  m.w.e. rock shielding against cosmic muons, reducing the vertical muon rate to  $4.5$  /day/m<sup>2</sup>. The 320 g germanium detectors are operated at a very low temperature (typically 17 mK) within a dilution cryostat. This cryostat, made mostly of ultrapure copper, is further protected from external radioactivity by 10 cm Cu and 15 cm Pb shields [3]. Pure nitrogen gas is circulated inside this shielding to reduce radon accumulation. An external 30 cm layer of paraffin protects the experiment from neutrons created in the rock. Inside the cryostat, the detectors are shielded from the radioactivity in components of the electronics by 7 cm of roman lead <sup>1</sup>. The cold electronic components (in total, nine FETs and a dozen of resistors and capacitances) are kept as far away as possible from the detectors, and the rest of the acquisition chain remains outside the cryostat. Fig. 1 presents a schematic cut view of the cryostat inside its Cu and Pb shields.

---

<sup>1</sup>The archeological lead comes from an antique roman ship. The wreck was investigated during four campaigns (1984-86) supervised by M. L'Hour of the Direction des Recherches Archéologiques Sous-Marines [4].

The detectors themselves are encased into 1 mm thick ultrapure Cu casings, and held in place with the help of teflon balls and three small Cu springs (see the inset in Fig. 1). The thermal sensor consists of a small ( $1 \text{ mm}^3$ ) Neutron Transmutation Doped (NTD) germanium crystal glued directly onto each crystal. The thermal coupling to the cryostat is assured by ultrasonic bonding of several micrometric gold wires on gold pads. Electric connections are assured by the same kind of gold wires linking the electrodes to contact tracks on the copper casing. The wires going up to the 4 K pre-amplifier level are low radioactivity coaxial cables. Further details can be found in [5].

## 2.2 Active background rejection capabilities

It is impossible to completely shield the detectors from external radiation. Most of the radiation reaching the detectors is in the form of gamma rays. In EDELWEISS-I, the rate of gamma interactions exceeds the one expected from WIMPs by at least a factor  $10^5$ . In order to address this, the EDELWEISS detector technology offers means to actively discriminate between electron recoils caused by photons and electrons, and nuclear recoils caused by neutrons or WIMPs. Indeed, for the same interaction energy, nuclear recoils have an ionization efficiency on average three to four times less than electron recoils, depending on the energy [6]. By measuring simultaneously a heat signal and an ionization signal and considering the ratio of both parameters, it is possible to reject more than 99.9 % of the gamma interactions while keeping a 90 % efficiency for nuclear recoils down to an energy of 15 keV [2]. The value of this threshold depends on the experimental resolutions, which have been as low as 1.0 keV on the ionization channel and 0.3 keV on the heat channel.

The ionization measurement is made possible by two aluminum electrodes (thickness 60-100 nm) deposited onto top and bottom surfaces of the germanium detector. By applying a moderate voltage between the electrodes, charge carriers created by an interaction can be collected and give rise to a signal. The selected voltage is 4 V, which is high enough to efficiently collect charges but not too high in order to preserve the discrimination capabilities. Furthermore, one of the collection electrodes is actually separated into a center part and an outer guard ring (see Fig. 2). This allows to define a fiducial volume inside the detector where a reliable charge collection is expected, as opposed to the lateral sides where electric field lines can escape the crystal before they reach the electrodes, leading to an incomplete charge collection. The current NTD bolometer technology has been "upgraded" with the addition of a  $\sim 60 \text{ nm}$  layer of amorphous Ge (GGA detector type) or Si (GSA detector type) just below the electrodes (see Fig. 2), which essentially gets rid of the majority of surface interactions [7, 8].

## 3 Gamma background

### 3.1 Radioactivity measurements and material selection

More than 99.5 % of the interaction rate in the EDELWEISS-I detectors is due to gamma events. The 15 cm thick lead shield stops most of the gammas from outside the experimental setup and the observed gamma background comes from

the inside. To select low activity materials a separate low-background counting facility was built: a n-type coaxial High Purity Ge diode of 210 cm<sup>3</sup> operated at 77 K with archeological lead shielding. This dedicated HPGe diode was not set up at the time of construction of the shielding and of the cryostat. Thus, only a partial material selection could be performed before the experiment; the copper used for the shielding had to be measured “a posteriori”. The HPGe diode was intensively used for internal material selection close to the detectors. Table 1 displays the measured radioactivities of some components of the EDELWEISS-I set-up, most of them situated in the immediate vicinity of the detectors: copper detector holders, copper springs, teflon pads and coaxial cables.

### 3.2 Data sets and high-energy data reconstruction

The present analysis is based on two data sets. The first is the run labeled 2003p in Ref. [2], representing 39.4 kg.d of data (total volume of the three detectors) taken in very stable conditions, with similar performances of the three detectors in terms of energy threshold and recoil energy resolution. For the WIMP search, the amplifier gains, ADC bit ranges and channel sensitivities are optimized for the low-energy WIMP signal, with the consequence that ionization signals above 1 MeV saturate the digitizers. Saturation of the heat signal occurs at 350 to 600 keV, depending on the detector. This is far above the expected range for WIMP signals, but it affects the identification of radioactive backgrounds where gamma lines up to 2.6 MeV can prove useful.

For this reason, a dedicated run, labeled 2003h, has been recorded in the same experimental conditions as the run 2003p, but with all amplifier gains reduced by a factor 10. The total exposure for this run is 9.3 kg.d in the total volume of the three detectors.

Comparing the data from the runs 2003p and 2003h, it was confirmed that the saturated signals of the run 2003p could be corrected and their amplitudes could be calibrated reliably. This is possible because, as described in Ref. [2], extensive samples of the signal time profiles associated to each event are stored onto disk. However, the filtering applied by the acquisition system distorts the shape of saturated pulses. Therefore new templates were built by filtering ideal events truncated at different levels of saturation. The template used for a given event is the one giving the best fit. It is obtained by varying the saturation level of the template and minimizing the corresponding  $\chi^2$ .

This allowed us to reconstruct gamma and alpha events with recoil energies as high as 7 MeV, and a full width resolution of about 3 % at 2.6 MeV (ionization channel). This reconstruction method suffers however from a lack of sensitivity in the case of weakly saturated pulses as the procedure is comparatively more sensitive to the baseline level of the events which has a direct impact on the saturation level at a given energy. Conservatively, as discussed in [9], the method is not used below 1 MeV for the ionization channel, and below 350-600 keV for the heat channel, depending on the detector.

### 3.3 Experimental gamma background spectrum

The energy calibration of ionization signals was performed using <sup>57</sup>Co (122 keV), <sup>137</sup>Cs (662 keV) and <sup>60</sup>Co (1173 and 1332 keV) sources. The full width

resolution was about 2.5% and the response of the ionization channel was linear up to 1332 keV.

Fig. 3-a shows the ionization spectrum corresponding to the total volume of the three detectors for the two data sets 2003h (9.3 kg.day) and 2003p (39.4 kg.day). In these spectra, the 2003p data above 1 MeV have been reconstructed as described in the previous section. As we are concerned with the gamma spectrum, the alpha events, which appear with low quenching values essentially below 2 MeV ionization energy, have been eliminated by a cut on the quenching factor  $Q(Q < 0.5)$ , see below section 4. The most noticeable feature is a Compton backscattering bump around 200 keV. Lines originating from U-Th series are visible, notably the  $^{208}\text{Tl}$  line at 2614 keV with a full width resolution of about 3%. A peak of  $^{40}\text{K}$  at 1461 keV is also present.

### 3.4 Background simulations

Monte Carlo simulations are performed under GEANT3 [10] using the geometry given in Fig. 1 and the measured activities or limits of Table 1. Several sources of gamma background are successively studied and comparisons with the observed spectrum are given in Fig. 3-b to 3-d.

#### 3.4.1 Copper detector holders and thermal shields

The most massive materials in the immediate vicinity of the detectors are detector holders, cryostat structure and thermal shields. They are made of about 20 kg of ultra-pure copper (OFHC copper, purity > 99.99%). The upper limit on their U/Th content is 0.1 ppb (Table 1). After machining, the copper holders were brought underground only a few months before the start of the experiment. Therefore, the cosmogenic activation of  $^{60}\text{Co}$  (half-life 5.3 y) at the surface has to be considered. The experimental limit on  $^{60}\text{Co}$  is compatible with an equilibrium concentration of about 1 mBq/kg [11]. The U-Th and  $^{60}\text{Co}$  contributions, assuming activities equal to the limits, are compared in Fig. 3-b with the experimental spectrum. The simulated continuum is too low by one order of magnitude, with much more pronounced lines than actually observed.

#### 3.4.2 Radon

In the lead-copper shield, near the detectors, about 20 liters of air are trapped (see Fig. 1). Although continuously flushed with pure nitrogen emanating from the liquid nitrogen dewar, this volume is a potential source of radon contamination. No radon concentration measurement has been made and the decay of  $^{220}\text{Rn}$  is simulated assuming an activity of 10 Bq/m<sup>3</sup>, the mean value measured in the LSM cavity. As can be seen on Fig. 3-c, the simulated continuum is again much too low, and the predicted lines are not observed. Even with an unrealistic high concentration, the decay of radon can't account for the observed spectrum.

#### 3.4.3 Copper shield

The inner 10 cm thick copper shield (Fig. 1), is made of about 1 ton of copper bricks (electrolytic copper, 99.9% purity), purchased and brought underground in the early nineties. Measured "a posteriori", this copper shows a small but

measurable contamination in U-Th series (Table 1). The cosmogenic  $^{60}\text{Co}$  is, as expected, not detected after about two half-lives of decay underground. The simulation shows that the U-Th content of this copper shield accounts for most of the features of the background energy spectrum (see Fig.3-d). Gammas originating from the bulk of this copper shield go through several centimeters of material before they reach the detectors, and, as a consequence, lines aren't very pronounced, Compton diffusion being the dominant energy dissipation process above  $\sim 150$  keV. The Compton backscattering bump around 200 keV is reproduced though the lower amplitude in the simulation indicates that another source of high energy gamma rays might be present. The rate of the  $^{208}\text{Tl}$  line at 2614 keV ( $1.1\pm 0.2$  counts/kg/d) is reproduced within 30% by the simulation, a satisfying agreement given the uncertainty of 60% on the measured thorium concentration in copper.

#### 3.4.4 $^{40}\text{K}$

A peak of  $^{40}\text{K}$  at 1461 keV ( $1.6\pm 0.5$  counts/kg/d) is present in the energy spectrum. Table 1 shows that the highest  $^{40}\text{K}$  activity is found in the wires to the detectors (teflon sheath), but the involved mass is very low (few grams) and the simulated rate is two orders of magnitude lower than the observed one. The same holds for  $^{40}\text{K}$  contaminations of Cu springs (1.3 g for one detector) and teflon balls (0.4 g for one detector) in the detector holders. The present measurement of the copper of the gamma shield provides only an upper limit (Table 1), corresponding to a rate of 3.5 counts/kg/d in the  $^{40}\text{K}$  peak, which is consistent with the measured one (Fig. 3-a).

#### 3.4.5 Summary

Radioactivity measurements and associated simulations have shown that most of EDELWEISS-I gamma background arises from a tiny U/Th contamination of the very massive copper shield rather than from radioactive contaminations close to the detectors.

## 4 Backgrounds from alpha particles and surface events

### 4.1 Alpha particles

One of the most noticeable features revealed in the 2003h data is the presence of a distinct population localized at a recoil energy  $E_R = 5.33 \pm 0.03$  MeV with a quenching factor <sup>2</sup>  $Q = 0.30 \pm 0.02$ , consistent over the three detectors (see Fig. 4). This population was later confirmed in the 2003p data using the high-energy reconstruction procedure detailed in section 3.2 (see Ref. [9]). The rates vary from  $2.4 \pm 0.6$  to  $5.0 \pm 0.8$  counts/kg/d in the fiducial volumes (center electrodes) of the three detectors, and from  $13 \pm 2$  to  $25 \pm 2$  counts/kg/d in the lateral volumes (guard electrodes). We observe a significantly higher rate in the

---

<sup>2</sup>The quenching factor is defined as the relative ionization efficiency between a nuclear recoil and an electron recoil of the same real recoil energy.

top detector than in the bottom detector (Table 2), a fact for which we have no explanation.

Given the energy range and peculiar value of the quenching factor, we link this population to the interaction of alpha particles in our detectors. Our explanation is that the detectors themselves and/or their close environment, i.e. their copper holders, suffer from a  $^{210}\text{Pb}$  contamination. This isotope, with a half-life of 22.3 years, is a daughter of  $^{222}\text{Rn}$ . It can be implanted on a surface exposed to an atmosphere containing radon during the fabrication and handling of the detectors. The last disintegration of the chain  $^{210}\text{Pb} \rightarrow ^{210}\text{Bi} \rightarrow ^{210}\text{Po} \rightarrow ^{206}\text{Pb}$  produces an alpha with an energy of 5.3 MeV. If the events with  $Q < 0.5$  on Fig. 4 are interpreted as alphas, their energy spectrum restricts their origin to either the detectors themselves or the copper surfaces ( $\leq 1\mu\text{m}$ ) surrounding them. Indeed, given the very low penetration length of alpha particles of such energies in germanium or copper ( $\sim 10\mu\text{m}$ , see Table 3), a volume contamination of any material other than the germanium itself would undoubtedly lead to the observation of an alpha energy continuum down to 0 MeV. While we do observe such a tail to low energies, it is clearly not the dominant feature.

The localization in quenching is also interesting. Although such a phenomenon may be associated with incomplete charge collection due to surface interactions, it is difficult to explain why we observe a constant value of  $Q \sim 0.3$ , and not a range of values down from  $Q = 1$ . Previous studies [14, 15] have shown that charge collection efficiency for alpha interactions in Ge is similar to that of gammas. However, those measurements were obtained at room or liquid nitrogen temperatures, and under a drifting field of several thousands V/cm. Despite the lack of more relevant results, it is not unreasonable to assume that, in our case, because of the particular nature of an alpha interaction in germanium and the high local density of charges created, some systematic recombination before collection takes place. This would typically lead to a constant value of the quenching ratio, as is observed in our data.

## 4.2 Heavy nuclear recoils

When  $^{210}\text{Po}$  decays to  $^{206}\text{Pb}$  a 5.3 MeV alpha is produced and the  $^{206}\text{Pb}$  nucleus recoils with a kinetic energy of 103 keV. Depending on whether this takes place at the surface of the detector itself or at the surface of the copper in front of the germanium, what we expect to see is substantially different. In both cases, the penetration length of such a heavy particle at such a low energy is so small (a few tens of nm) that all of the ionization signal is lost, charges being absorbed either in the aluminum electrode (100 nm) or in the amorphous sub-layer (another 60 nm) if the Pb nucleus hits a surface not covered by an electrode. If the contamination is localized on the surface of the detector, the heat signal should correspond to the full recoil energy of 103 keV. In contrast, if the Pb nucleus originates from the copper, then it has to go through a thickness of material equivalent to its implantation depth before it reaches the detector, resulting in a partial loss of energy.

In order to isolate this heavy recoil population, we looked at all the events in our data compatible with a signal above detection threshold on the heat channel, and below threshold on the ionization channel. This led to a classification into three categories: a) sensor "NTD" events, induced inside the small thermal sensor by its own radioactivity; b) random noise events, linked



for example to anomalous microphonic episodes inside the cryostat, and c) "legitimate" ionization-less events, among which potentially lie the heavy recoils we seek. As described in Ref. [2], NTD events present a very particular pulse shape, significantly shorter than regular bulk events. We use shape discrimination to eliminate populations (a) and (b) and isolate population (c) (see Ref. [9] for details).

Using the data from run 2003p, in each detector we find a population of events clearly contained below 100 keV (Fig. 5), with rates varying from  $1.5 \pm 0.5$  to  $5.4 \pm 0.8$  counts/kg/d in the total volume of the detectors for recoil energies greater than 40 keV (see Table 2). Interestingly, as was the case with alpha interactions, the top detector registers more events than the bottom one, and in the same ratio within the error limits. This tends to confirm that both populations are indeed linked. The fact that we do not see a clear peak at 103 keV but a roughly uniform front below this energy also implies that the contamination is localized exclusively on the copper surfaces, and not on the detectors themselves.

### 4.3 Surface beta interactions

If the contamination is indeed linked to an exposure to radon, then we expect to see the products of all disintegrations in the  $^{210}\text{Pb}$  chain, in addition to the 5.3 MeV alphas and heavy recoils. In particular, the  $^{210}\text{Pb}$  decay to  $^{210}\text{Bi}$  leads to a complex spectrum of low energy conversion and Auger electrons together with two beta spectra with end-points at 63.5 keV and 17 keV. Due to the value of its penetration length in germanium (see Table 3), the 46.5 keV gamma ray does not contribute significantly to the surface event budget. The decay of  $^{210}\text{Bi}$  to  $^{210}\text{Po}$  emits another beta electron (branching fraction 100%) with an end-point of 1.16 MeV.

According to Monte-Carlo simulations using the CASINO code [12] (see Table 3), an electron of 100 keV impinging at normal incidence the germanium surface will lose 90% of its energy in the first 20  $\mu\text{m}$ . This value goes up to  $\sim 700$   $\mu\text{m}$  for a 1 MeV electron. As for the nuclear recoils (sect. 4.2), the 100 nm aluminum electrode and the 60 nm amorphous semi-conductor sub-layer constitute a "dead ionization zone" in our detectors. As for the alphas (sect. 4.1), there exists a zone under the electrodes where electron-hole pairs are not properly collected. The depth of this zone can be as large as 10  $\mu\text{m}$ , as studies using detectors with a different design have shown [7, 16].

We therefore expect to observe some incomplete charge collection for a significant part of the events generated by the decay electrons. In the 2003p data, we do indeed observe a population of "intermediate" events between the electron recoil band and the nuclear recoil band (Fig. 6). As shown in Ref. [2], this population is absent when the detectors are exposed to a  $^{137}\text{Cs}$  source of penetrating gamma rays. In order to quantify this population, we compare our low-background data to  $^{137}\text{Cs}$  gamma calibration data. This allows us to define an area in the  $(Q, E_R)$  plane (with  $E_R \leq 80$  keV) where we can be confident that events are not caused by gamma or neutron interactions with full charge collection [9]. This selection underestimates the actual total population of incomplete charge collection events. In order to provide an order-of-magnitude estimate of the rate of surface betas, we assume a 50% selection efficiency as hinted by Fig. 13 of Ref. [2]. The results are given in Table 2: the count rates

are similar to those of alpha particles. Furthermore, the same ratios between the counting rates in each detector are observed. We also notice that the intermediate population appears to display energies below  $\sim 60$  keV, which is the maximum energy for an electron from a  $^{210}\text{Pb}$  beta decay. These observations point toward a correlation between the identified alpha population and this intermediate population.

#### 4.4 Contamination scenario

In conclusion, we have identified three event populations consistent with a single coherent contamination scenario:

- A population of alpha interaction events from the disintegration of  $^{210}\text{Po}$  very close to the detectors, with rates of the order of 5 counts/kg/d in the fiducial volumes of the detectors.
- A population of ionization-less events, with energies below 100 keV, which we can identify with  $^{206}\text{Pb}$  recoils originating from the copper surfaces facing the detectors. The count rates are of the same order as those observed for alpha interactions, and the rate ratios between detectors are consistent with alpha data.
- A population of events with ionization yields lying between those for gamma rays and those for nuclear recoils, associated to surface interactions, which we link to electrons emitted in the decay of  $^{210}\text{Pb}$ . Here again, the rates are of the same order as those observed for alpha interactions, and the ratios between detectors are conserved.

This leads us to strongly suspect the  $^{210}\text{Pb}$  contamination of the copper parts facing the detectors while the hypothesis of a contamination of our detectors themselves is not favoured due to the absence of registered ionization-less events with a nominal energy of 103 keV.

It is worth mentioning that the gamma component of the background produces also Compton electrons which can escape from the copper surfaces surrounding the detectors. Miscollected surface events can be produced when such low energy electrons hit a detector. The simulation of the dominant gamma background (from the bulk of the copper shield) has shown that, below 200 keV, 0.6 % (1.1 %) of the events are electrons interacting in the first 20  $\mu\text{m}$  (50  $\mu\text{m}$ ) under the electrodes; electrons coming from outside of the detectors constitute 70 % of these populations. The absolute rates are between 2 counts/kg/d (20  $\mu\text{m}$ ) and 4 counts/kg/d (50  $\mu\text{m}$ ), the actual fraction of miscollected electrons depending on the variation of the charge collection efficiency with depth.

Finally, a complete model of beta contamination on the detector and copper surfaces should also consider  $^{14}\text{C}$ . All surfaces are usually quickly covered by a thin (about 1.5-4 nm) layer of organic compounds  $\text{CH}_x$  (see for instance [17]). Given an isotopic ratio  $^{14}\text{C}/^{12}\text{C} = 1.3 \times 10^{-12}$ , this yields 0.5 to 3 beta electrons/kg/d for the central part of a detector, with a 156 keV end-point. Comparison with “intermediate event” rates given in Table 2 shows that there might be a contribution from  $^{14}\text{C}$  contamination.

## 5 Neutron background

Fast (0.5-10 MeV) neutron interactions are a dangerous background as they produce nuclear recoils that can mimic a WIMP signal. One coincidence between nuclear recoils in two detectors due to a neutron was observed in EDELWEISS-I data [2]. We present in this section the simulations of this neutron background.

### 5.1 Simulation of neutron transport in EDELWEISS-I

Before any attempt to evaluate the number of nuclear recoils in the EDELWEISS - I data due to interactions from a residual neutron flux, it is necessary to test the reliability of the Monte Carlo code used for neutron transport through a simulation of a calibration run with a  $^{252}\text{Cf}$  source. Using GEANT3 a normalization factor of 0.68 had to be applied to the simulation to reproduce the experimental rates [18]. An alternative simulation was then performed with MCNPX [19]. The detector response was applied to the simulated germanium recoils as described in Ref. [5]. The data and the simulation were then analyzed using the same selection procedure to extract the recoil energy spectra.

The  $^{252}\text{Cf}$  source was positioned, through a 50 mm diameter hole in the lead/copper shield, at 70 mm from the external wall of the lead shield and at 20mm below the detector stack: the neutron count rate decreased from the bottom (GGA3) to the top (GSA3) detector. These rates are well reproduced by the simulations as can be seen in Fig. 7. The ratio MCNPX/data of total number of events is  $1.067 \pm 0.079$  (measured activity of the source [18])  $\pm 0.015$  (Stat)  $\pm 0.007$  (MC Stat). The measured proportion of events in the 3 detectors of 27%, 32% and 40% is well reproduced by the simulation (30%, 32% and 40%). However the shapes of the energy spectra differ slightly, a feature also observed with GEANT3 simulations.

### 5.2 Neutron flux in the Modane underground laboratory

With a rock overburden equivalent to 4800 m of water, the residual neutron background originates mainly from the radioactivity of the rock. Two contributions arise from the contamination of U/Th: spontaneous fission and  $(\alpha,n)$  reactions. In Ref. [20], the neutron flux coming out of the LSM rock had been deduced from the measurements made with a  $^6\text{Li}$ -doped liquid scintillator cell, using GEANT3 for the neutron transport simulation. This spectrum was in turn interpreted in terms of the sum of the contributions from spontaneous fission and  $(\alpha,n)$  reactions, using a simplified calculation for the latter process. In Ref. [21], the original data had been re-interpreted in the light of more reliable neutron transportation codes (optimized versions of GEANT3 and MCNPX), having for consequence the reduction of the estimated neutron flux in the LSM from  $4.0 \cdot 10^{-6}$  to  $1.6 \cdot 10^{-6}$  n/cm<sup>2</sup>/s. In the present work (first introduced in Ref. [22]), we conclude these studies by using the SOURCES [23] code, which includes a more exact calculation of the  $(\alpha,n)$  contribution and using MCNPX for neutron transport.

The neutron flux in the LSM was simulated using the procedure described in [24]. The SOURCES code was used to calculate the rate and energy spectrum of neutrons produced by spontaneous fission and  $(\alpha,n)$  reactions due to the U/Th contamination in the rock. The LSM rock composition and its U/Th

contamination was taken from Ref. [20]. The neutron propagation in the rock to the LSM cavity takes into account backscattering on the walls. In the present calculation, the concrete covering the walls is not present.

The measurement of Ref. [20] was performed with a  $^6\text{Li}$ -doped NE320 liquid scintillator cell, where neutrons were positively identified from the observation of a proton recoil followed by the neutron absorption on  $^6\text{Li}$ . The detector ( $8.5 \times 8.5 \times 85 \text{ cm}^3$  scintillator) and its shielding (5 cm Cu and 12 cm Pb) were simulated with the MCNPX code. The detection efficiency is about 10% for incident neutrons above an energy threshold of 2 MeV. The following treatments were applied: light yield efficiency based on Birks' law fitted to proton data, 10% energy resolution, 43% event selection efficiency [20].

Fig. 8 shows the comparison of the simulations to the data. The SOURCES spectrum agrees better in shape with the data than the spectrum determined in Ref. [20]. Note however that all simulations are normalized to data. A normalization factor of 2.28 is needed in the simulation, which could be explained by inhomogeneities in the rock composition of the LSM walls, especially its water content. The large influence over the neutron flux of a small amount of hydrogen (mainly in water) in the LSM rock is emphasized in Ref. [24]: the 1% hydrogen content reduces the neutron flux above 1 MeV by a factor 2.1 (see also Ref. [25] for a discussion of this effect in the Gran Sasso context).

Fig. 9 shows the results of the simulation for the neutron spectrum in the LSM cavity after normalization to the data. We take the normalization factor as a systematic uncertainty on the simulation. We obtain a flux of  $1.06 \pm 0.10(\text{stat.}) \pm 0.59(\text{syst.}) 10^{-6} \text{ n/cm}^2/\text{s}$  above 1 MeV. Assuming a full coverage of the walls by concrete and its U/Th contaminations taken from Ref. [20] would give essentially the same result on the flux (less than 1% higher) with a corresponding normalization factor of 2.03.

### 5.3 Neutrons in EDELWEISS-I

The rate of nuclear recoils due to the neutron flux coming out of the rock, as estimated in Fig. 9, has been calculated using MCNPX. This flux is transported through the 30 cm paraffin shielding and the experimental setup shown in Fig. 1.

We expect about  $0.026 \pm 0.002(\text{MC stat}) \pm 0.018(\text{syst})$  neutrons/kg/d from the rock radioactivity,  $0.002 \pm 1.2\%$  (MC stat) neutrons/kg/d from the 0.25 ppb  $^{238}\text{U}$  contamination of copper shield and less than 0.001 neutrons/kg/d from the upper 0.1 ppb limit on  $^{238}\text{U}$  contamination in lead shield. This translates into about  $1.6 \pm 0.1(\text{MC stat}) \pm 1.1(\text{syst})$  nuclear recoils expected in EDELWEISS - I data (62 kg·day). Fig. 10 shows the corresponding recoil spectra in the detectors. The experimental spectrum of Ref. [2], with 34 events between 15 and 30 keV and 3 between 30 and 100 keV, can easily accommodate the presence of a few nuclear recoils due to neutron scattering. The only direct experimental proof of the presence of a neutron flux is the observation of a coincidence between nuclear recoils in two detectors [2]. The present simulation gives further support for this interpretation. First, the rock spectrum of Fig. 10 shows that the recoil energies in this coincidence (14.8 and 14.5 keV) are typical for neutron scattering. Secondly, the simulation confirms that the ratio of single to coincidence is approximately 10:1, consistent with the ratio observed in neutron calibrations. With this ratio, it was concluded in Ref. [2] that from one coincidence, the prediction range for accompanying single events is from zero to

40 events at 90% CL. Although consistent with the hypothesis of a background originating from both surface events and neutron interactions, this range does not help constrain the relative importance of these two contributions.

## 6 Conclusions and prospects

Three main backgrounds have been identified in the EDELWEISS-I data sets. The sensitivity is limited by background events which, after the nuclear recoil selection, mimic true WIMP induced nuclear recoils with a low value, about 0.3, of the ionization to recoil signals ratio  $Q$ . EDELWEISS-II, the second phase of the experiment, is designed for a two orders of magnitude sensitivity improvement relying upon the efficient rejection of these background events.

Before the rejection of the bulk electron recoils, the overwhelming majority of the events is a gamma population entirely dominated by the U/Th contamination of the Cu shield. These events are rejected with an efficiency greater than 99.9%. Nevertheless Compton electrons can escape from the closest copper surfaces, reach the detectors and possibly produce miscollected surface events; the gamma component has then to be maintained as low as possible. In the EDELWEISS-II set up, extensive material selection, mounting and operation of the cryostat under clean room conditions (class 100), secure a better radioactive cleanliness. Copper is no longer used for shielding. The inner part of the shield is made of very low radioactivity archeological lead. Based on GEANT3 simulations and the results of the activity measurements, the overall gamma rate for this new setup is predicted to be between 1.0 and 0.1 of the gamma rate of EDELWEISS-I, using upper limits or central values, respectively.

A very small  $^{210}\text{Pb}$  contamination at the surface of the copper detector casings is the very likely source of the observed alphas and near-electrode electron events showing a deficit of the charge collection. This probably comes from an exposure to radon at some steps of the manufacturing and handling process. In order to minimize the radon exposure, the EDELWEISS-II clean room is supplied, during the detector mounting phase, with air of very low radon concentration delivered by the LSM radon-trap facility. Nevertheless a more decisive approach consists in the identification and rejection of the near-surface events. Detectors equipped with  $\text{Nb}_x\text{Si}_{1-x}$  thin films as thermal sensors have been operated in the last months of the EDELWEISS-I phase. These films are sensitive to the transitory athermal part of the phonon signal, which constitutes a near-surface tag [26]. These first tests with 200 g modules have shown a factor of ten reduction of the surface event rate while retaining a 80% efficiency. Seven 400g NbSi modules, over a total of 28 detectors, will be operated in the first phase of EDELWEISS-II. Other possible solutions are still in a R&D phase: identification of surface events using interdigitized electrodes or pulse shape analysis of the charge signal [27].

The last identified background component comes from neutrons, which, as WIMPs, induce nuclear recoils through elastic scattering. The corresponding count rate is not yet much constrained by EDELWEISS-I, but its existence is established by the observation of one coincidence event. For EDELWEISS-II the reduction of this neutron background becomes critical. A 50 cm thick polyethylene shield all around the experiment moderates the low energy neutrons. Neutrons created by muon interactions in the shielding are tagged with

a 5 cm thick plastic scintillator muon veto of 100 m<sup>2</sup> surrounding the whole experiment (95% coverage). The compact arrangement of the multi (up to one hundred) detector structure allows further rejection through anti-coincidence between detectors.

EDELWEISS-II is now running at the Laboratoire Souterrain de Modane and first results are scheduled for 2007.

## Acknowledgments

The help of the technical staff of the Laboratoire Souterrain de Modane and of the participant laboratories is gratefully acknowledged. This work has been partially supported by the EEC Applied Cryodetector network (Contracts ERBFM-RXCT980167 and HPRN-CT-2002-00322) and the ILIAS integrating activity (Contract RII3-CT-2004-506222).

## References

- [1] R. J. Gaitskell, *Ann. Rev. Nucl. Part. Sci.* 54, 315 (2004)
- [2] V. Sanglard *et al*, *Phys. Rev. D* 71, 122002 (2005).
- [3] A. de Bellefon *et al*, *Astropart. Phys.* 6, 36 (1996).
- [4] M. L'Hour, *Rev. Archeol. Ouest* 4, 113 (1987)
- [5] O. Martineau *et al*, *Nucl. Instrum. Methods Phys. Res. A* 530, 426 (2004).
- [6] J. Lindhard *et al*, *K. Dan. Viderask. Selsk., Math. Fys. Medd.* 33, 10 (1963) and 36, 10 (1968).
- [7] T. Shutt *et al*, *Nucl. Instrum. Methods Phys. Res. A* 444, 340 (2000).
- [8] A. Benoit *et al*, *Phys. Lett. B* 545, 43 (2002).
- [9] S. Fiorucci, Thèse de doctorat de l'Université Paris-XI Orsay (2005). Available from: <http://edelweiss.in2p3.fr>
- [10] R. Brun *et al*, GEANT3, publication DD/EE/84-1, CERN (1987)
- [11] G. Heusser, *Proceedings of the Third International Summer School on Low Level Measurements of Radioactivity in the Environment*, World Scientific, 69 (1994).
- [12] CASINO software, <http://www.gel.usherb.ca/casino/>
- [13] SRIM software, <http://www.srim.org>
- [14] K.G. McKay and K.B. McAfee, *Phys. Rev.* 91, 5 (1953)
- [15] H. V. Klapdor-Kleingrothaus *et al*, *Proceedings of the third International Conference on Dark Matter in Astro and Particle Physics - DARK2000*, Springer, 553 (2000). arXiv:hep-ph/0103082.
- [16] D. S. Akerib *et al*, *Phys. Rev. D* 72, 052009 (2005).
- [17] A. Špalek *et al*, *Nucl. Instrum. Methods Phys. Res. B* 196, 357 (2002)

- [18] V. Sanglard, Thèse de doctorat de l'Université Claude Bernard Lyon 1 (2005).
- [19] Simulation code MCNP, <http://laws.lanl.gov/x5/MCNP/>
- [20] V. Chazal *et al*, *Astropart. Phys.* 9, 163 (1998).
- [21] G. Chardin and G. Gerbier, *Proceedings of the 4th Int. Workshop on Identification of Dark Matter*, World Scientific Singapore, 470 (2003)
- [22] R. Lemrani and G. Gerbier, *Proceedings of the Ninth Int. Conf. on Topics in Astroparticle and Underground Physics (TAUP 2005)*, J. Physics: Conf. Series 39, 145-147 (2006).
- [23] W. B. Wilson, SOURCES-4A *Los Alamos National Laboratory Report* LA-13639-MS, 1999.
- [24] R. Lemrani *et al*, *Nucl. Instrum. Methods Phys. Res. A* 560, 454 (2006)
- [25] H. Wulandari *et al*, *Astropart. Phys.* 22, 313 (2004).
- [26] A. Juillard *et al*, *Proceedings of the 11th International Workshop on Low Temperature Detectors (LTD-11)*, *Nucl. Instrum. Methods Phys. Res. A* 559, 393, 2006.
- [27] A. Broniatowski *et al*, *Proceedings of the 11th International Workshop on Low Temperature Detectors (LTD-11)*, *Nucl. Instrum. Methods Phys. Res. A* 559, 378, 2006.

	U (ppb)	Th (ppb)	<sup>40</sup> K (mBq/kg)	<sup>60</sup> Co (mBq/kg)	<sup>210</sup> Pb (mBq/kg)
Copper shield	$0.25 \pm 0.06$	$0.44 \pm 0.27$	$< 15$	$< 0.6$	$300 \pm 150$
Copper holders	$< 0.1$	$< 0.1$		$< 1.0$	
Cub1 springs	$< 0.6$	$< 1.7$	$40 \pm 30$		$260 \pm 130$
Roman lead	$< 0.022$	$< 0.032$	$< 1.3$		$< 200$
Teflon balls	$< 0.2$	$< 0.5$	$80 \pm 30$	$5 \pm 2$	$40 \pm 20$
Wires			$1400 \pm 1000$		

Table 1: Measured contaminations or activities for several materials used in EDELWEISS-I. Statistical errors are at  $1\sigma$  and limits at 90% confidence level (the detector background at 46.5 keV leads to high errors on <sup>210</sup>Pb activities).

Detector Electrode	GSA3		GSA1		GGA3	
	Center	Guard	Center	Guard	Center	Guard
Alphas count rate (/kg/d)	$5.0 \pm 0.8$	$24.7 \pm 2.2$	$5.2 \pm 0.8$	$17.8 \pm 1.7$	$2.4 \pm 0.6$	$13.3 \pm 1.5$
Heavy nuclear recoils Count rate (/kg/d)	$5.4 \pm 0.8$		$2.1 \pm 0.6$		$1.5 \pm 0.5$	
"Intermediate events" Count rate (/kg/d)	$6.3 \pm 1.0$	$33.0 \pm 2.5$	$5.0 \pm 0.8$	$33.3 \pm 2.4$	$3.2 \pm 0.7$	$20.6 \pm 1.9$

Table 2: Count rates for alpha events, heavy nuclear recoil events (recoil energy greater than 40 keV) and "intermediate events" (between 15 and 200 keV recoil energy). These latter are defined as the events between the electron recoil band at  $3.29\sigma$  and the nuclear recoil band at  $1.65\sigma$  (see Fig. 6).

Particle	Energy	Cu	Ge	Pb
Gamma	10 keV	$9\ \mu\text{m}$	$170\ \mu\text{m}$	$18\ \mu\text{m}$
	100 keV	6 mm	8 mm	$400\ \mu\text{m}$
	1 MeV	40 mm	80 mm	30 mm
Electron	10 keV	200 nm	350 nm	
	100 keV	$11\ \mu\text{m}$	$20\ \mu\text{m}$	
	1 MeV	$340\ \mu\text{m}$	$700\ \mu\text{m}$	
Alpha	5.3 MeV	$11\ \mu\text{m}$	$19\ \mu\text{m}$	$15\ \mu\text{m}$
Polonium	100 keV	40 nm	68 nm	

Table 3: Typical penetration lengths of various particles in Cu, Ge and Pb. Values for gammas correspond to a 10 % transmission probability. Values for electrons correspond to the maximum depth at which an electron has deposited 90 % of its energy (results from CASINO [12] simulations). Values for alphas and Po nuclei are the mean penetration length given by SRIM [13] simulations with a normal incidence.



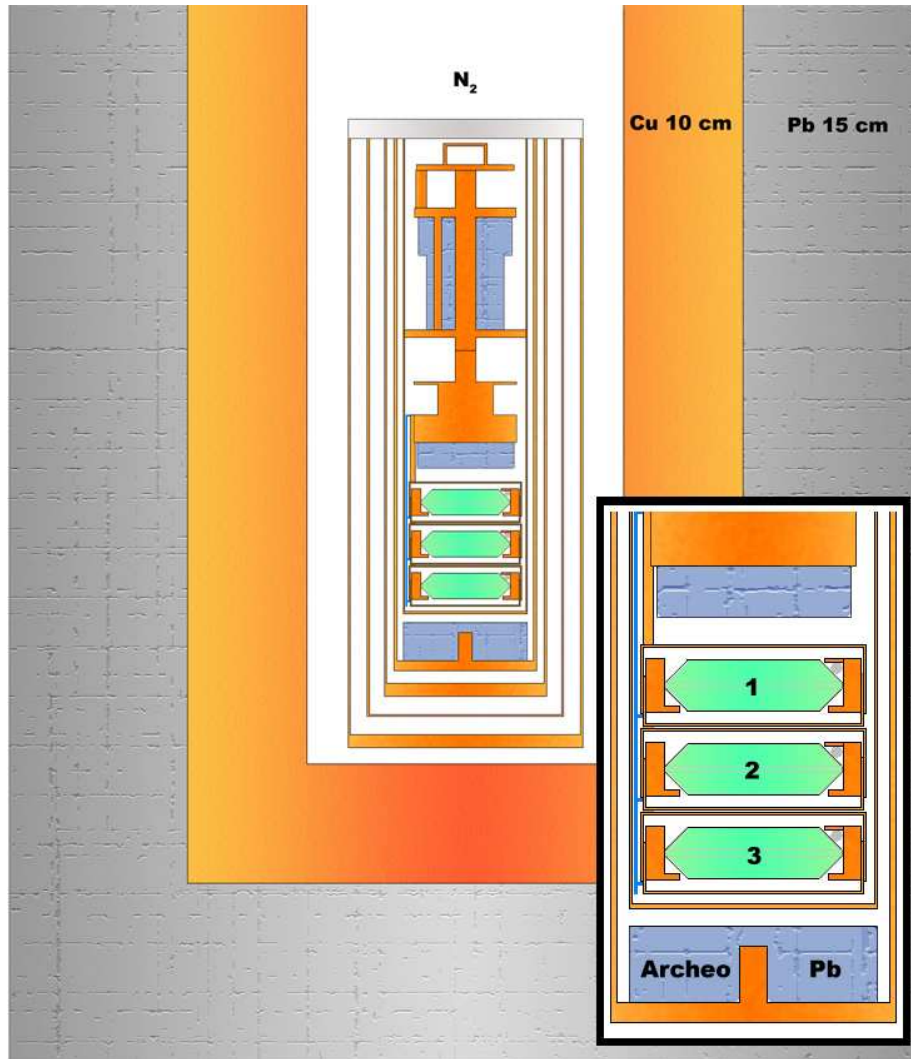


Figure 1: Schematic view of the EDELWEISS-I cryostat within its Cu and Pb shields, as implemented in GEANT3 Monte Carlo simulations. Orange areas figure copper, grey textured areas stand for lead. The inset shows the three germanium detectors (from top to bottom: GSA3, GSA1 and GGA3) encased into individual copper casings. Teflon balls and Cu springs are visible in the upper right corner of the detectors holders. Wires to the cold electronics are going up at the left of the detector stack. Not represented on the figure is the 30 cm external paraffin shield against neutrons.

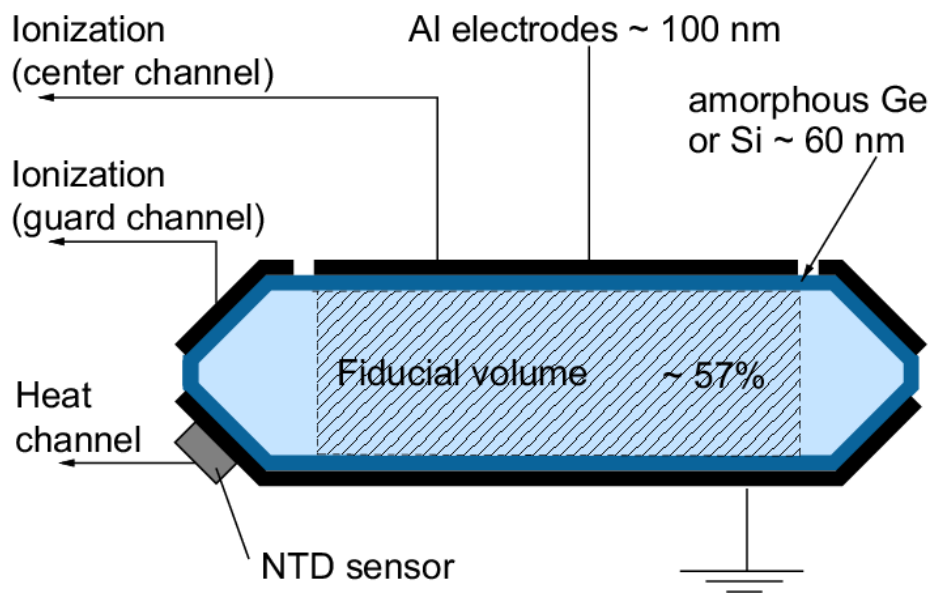


Figure 2: Schematic cut of an EDELWEISS heat and ionization germanium detector. The thickness of Al electrodes, amorphous layer and NTD sensor are not represented to scale.

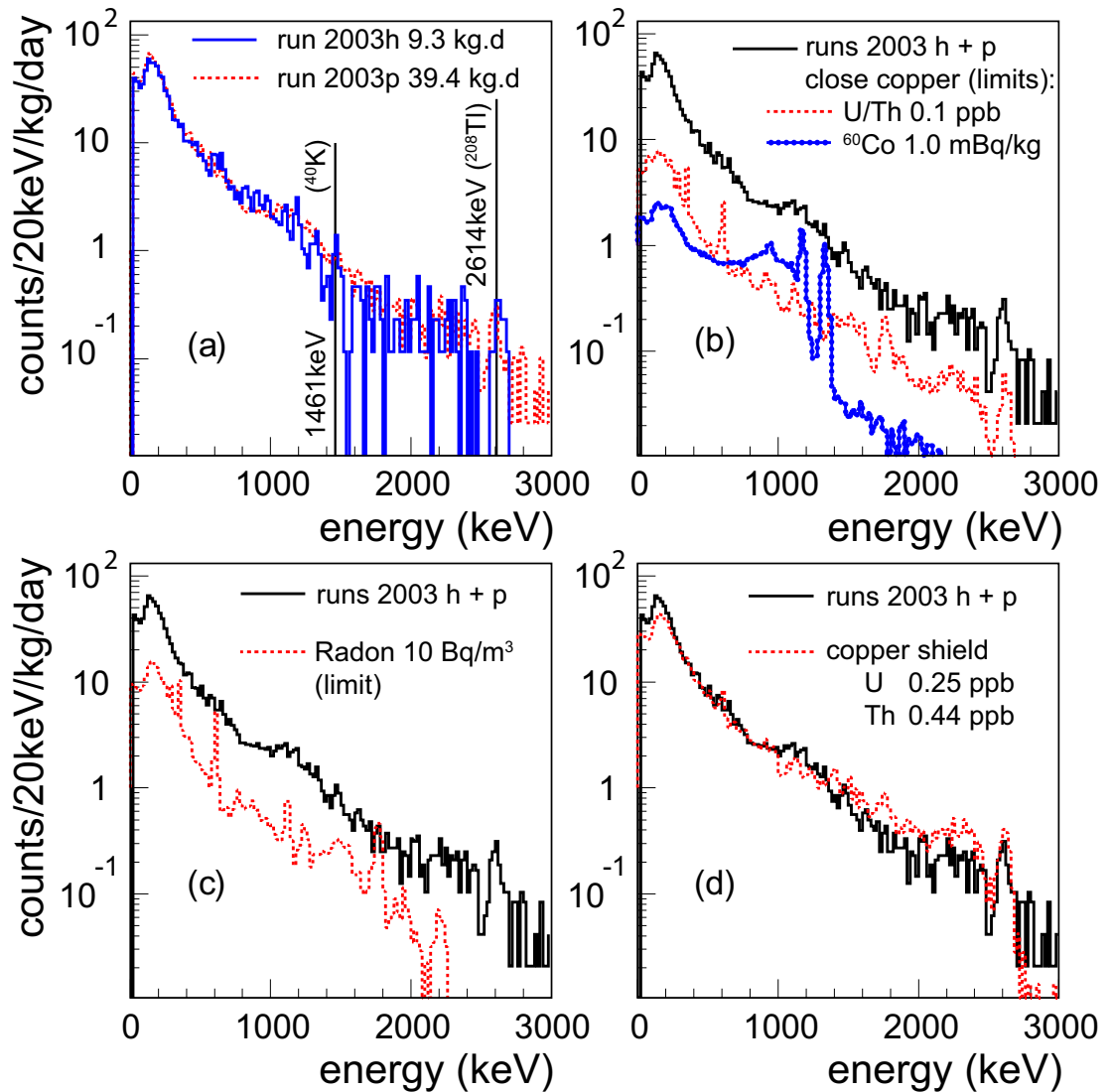


Figure 3: Gamma background energy spectrum (ionization channel) compared to Monte Carlo simulations of various sources of radioactive contamination. (a) The two experimental data sets 2003h (full line) and 2003p (dashed line). (b) Sum of the 2003p and 2003h data sets (full line), simulations of the U/Th (dashed line) and  $^{60}\text{Co}$  (dotted line) contents of copper close to the detectors (detector holders, cryostat). The quoted radioactive contaminations are measured upper limits. (c) Sum of the 2003p and 2003h data sets (full line), simulated contribution of the radon trapped in the lead-copper shield (upper limit, dotted line). (d) Sum of the 2003p and 2003h data sets (full line), simulation of the U/Th content of the copper shield (measured concentrations, dashed line).

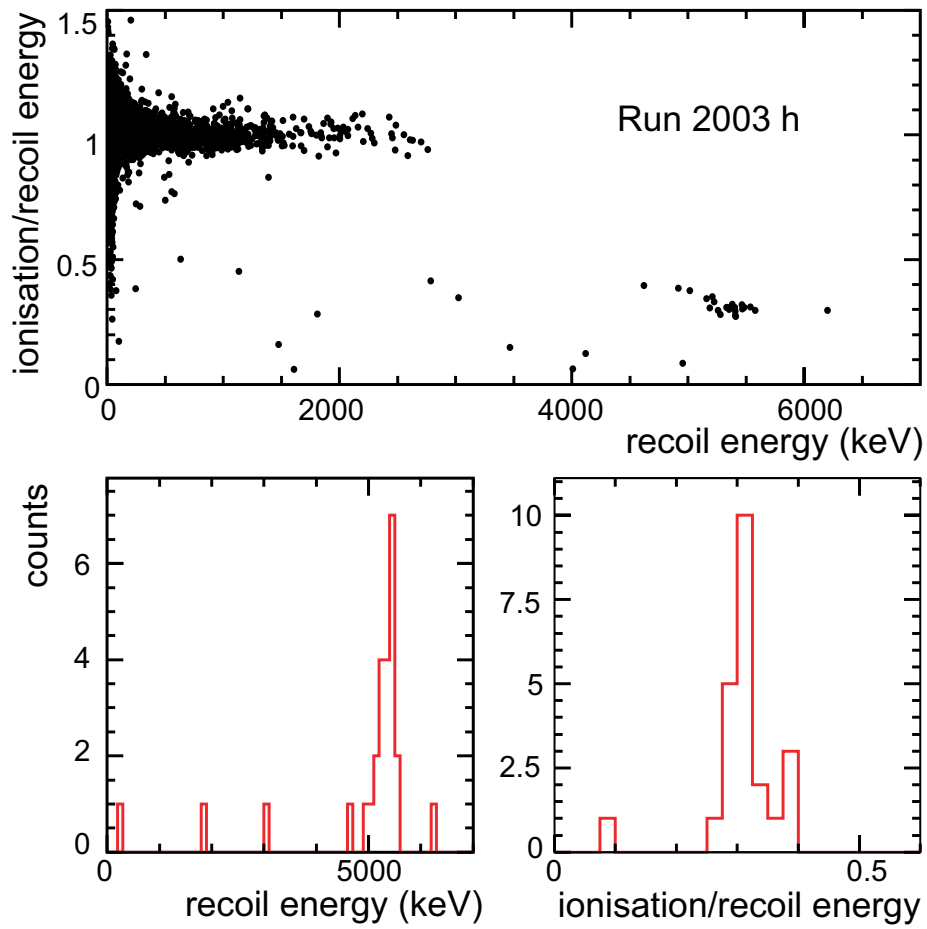


Figure 4: Distribution of the ionization quenching ratio  $Q$  with recoil energy  $E_R$ , for the data of the run 2003h. Bottom left:  $E_R$  projection for  $0.2 < Q < 0.4$ . Bottom right:  $Q$  projection for  $4.5 < E_R < 6$  MeV.

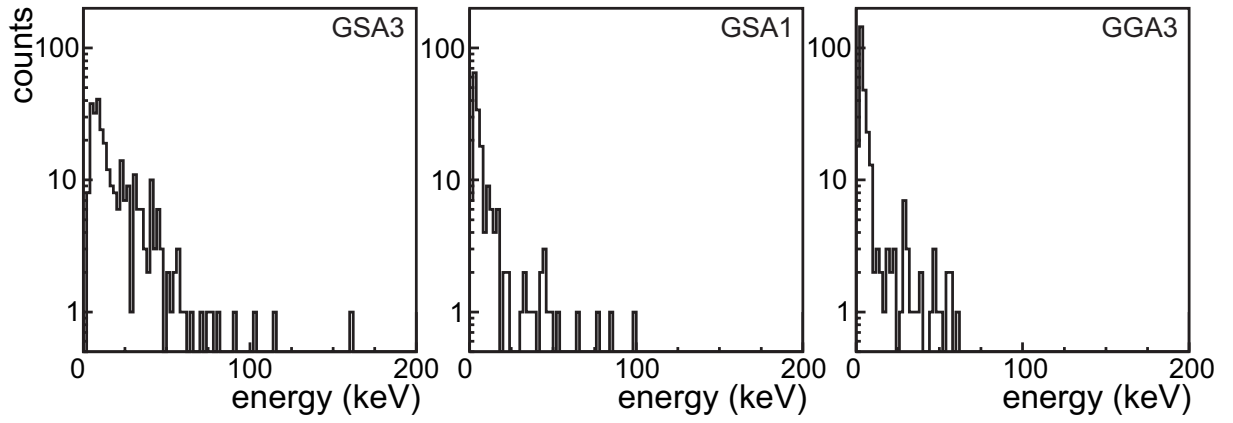


Figure 5: Amplitude distributions of ionization-less events after rejection of NTD events and noise events. The heavy nuclear recoil events at the surfaces belong to this population.

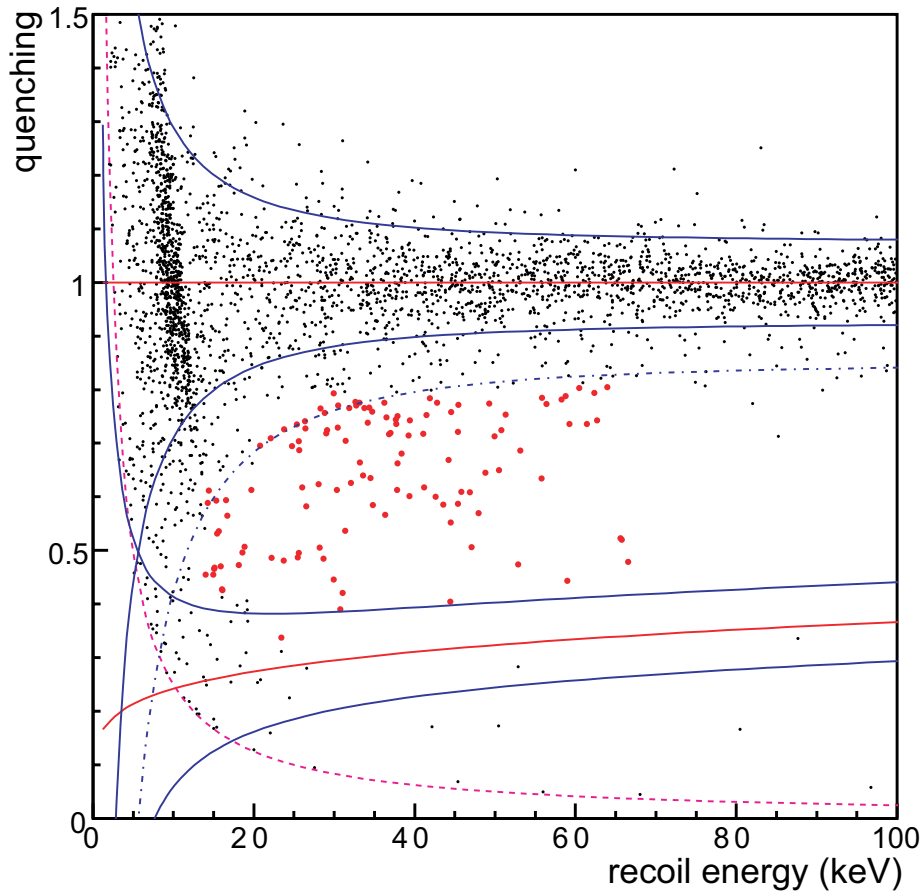


Figure 6: Representative sample of the “intermediate event” population: run 2003p, sum of the fiducial volumes of the three detectors, 22.5 kg.d. Full (red) circles: selected “intermediate events”; (black) dots: remaining part of the low background data.

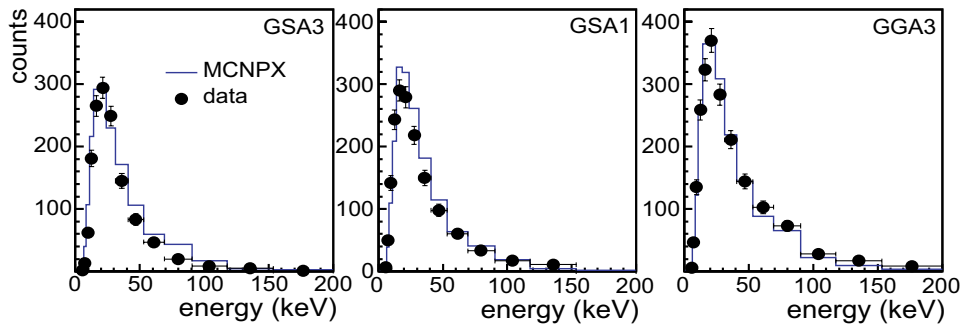


Figure 7: Energy spectra of the nuclear recoils in EDELWEISS-I calibration runs with a  $^{252}\text{Cf}$  neutron source. The MCNPX simulation is also shown (full line, no normalization to data).

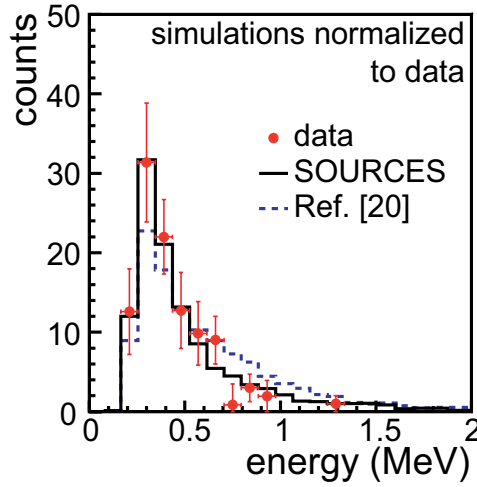


Figure 8: Neutron flux measurements in the LSM cavity from Ref. [20]. The data points are the experimental electron equivalent energy spectrum. The dotted line is the original simulated spectrum from rock radioactivity [20]. The full line corresponds to the present work using SOURCES and MCNPX. Both simulations are normalized to the data.

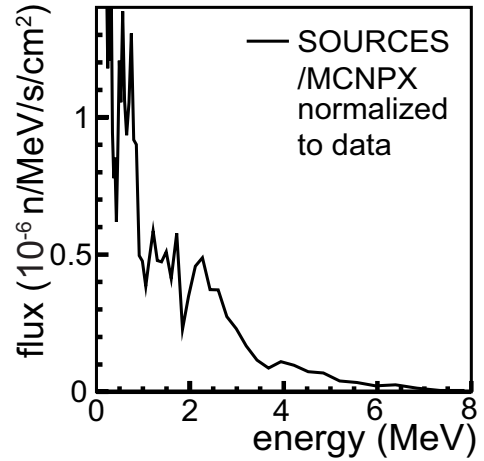


Figure 9: Simulated neutron energy spectrum in the LSM after normalization to data of Ref. [20]. The neutron production from  $^{238}\text{U}$  and  $^{232}\text{Th}$  traces in the rock is simulated with SOURCES and propagated with MCNPX.

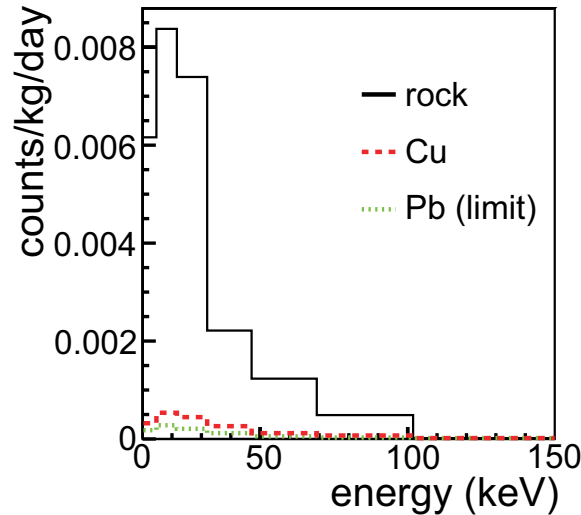


Figure 10: Expected energy spectra of the nuclear recoils in EDELWEISS-I low-background runs from radioactivity of the rock (full line),  $^{238}\text{U}$  contamination in copper (dashed line) and in lead (dotted line).